

Addition of *N*-(2-Aminoethyl)naphthalimide and Mercaptopropionic Acid to Increase the Stability of CsFAMA Perovskite Solar Cells

Raphael F. Moral,^{1b} Alden B. Hermsdorff,^a Paulo E. Marchezi,^a José C. Germino,^{a,b}
Luiz G. Bonato,^a Francineide L. de Araújo^{1b}*,^a and Ana F. Nogueira^{1b}*,^a

^aInstituto de Química, Universidade de Campinas, 13083-872 Campinas-SP, Brazil

^bDepartment of Physics, Institute for Nanostructures, Nanomodulation and Nanofabrication (i3N),
University of Aveiro, Aveiro, Portugal



Sustainable energy generation has been a growing concern worldwide due to the alarming effects of climate changes in the last few decades. In this scenario, perovskite solar cells hold great promise in contributing for a greener global energy matrix. Despite the great potential of this technology, several difficulties to deploy perovskite solar panels are yet to be overcome, being their long-term stability one of the most critical. In this sense, this work offers an alternative to improve the long-term, operational stability of the devices by passivating the CsFAMA perovskite active layer with a mixture of *N*-(2-aminoethyl)naphthalimide and mercaptopropionic acid. These modifications improved the perovskite and device stability under ambient conditions. The solar cells without encapsulation and with post-treatment with 5 mM modifier solution retained ca. 90% of its initial power conversion efficiency (PCE) after 500 h exposed to ambient conditions, while standard solar cells retained ca. 58%. Our approach offers a simple new method to improve the stability of perovskite solar cells using an unexplored combination of passivating molecules.

Keywords: perovskite solar cells, stability, *N*-(2-aminoethyl)naphthalimide synthesis, mercaptopropionic acid

Introduction

The climate change has been showing progressively more serious effects in recent years, and there has been a global effort in implementing a circular economy, especially concerning energy consumption and generation.^{1,2} During the last decade, perovskite solar cells (PSCs) have emerged as a promising technology for solar energy harvesting.³⁻⁵ In this short period of development, PSCs have achieved values of power conversion efficiency (PCE) above 25%, comparable with well-established technologies such as single-crystal-Si and polycrystalline-Si solar cells,^{6,7} with a special advantage: perovskite thin-films can be processed via wet protocols, enabling printed electronic and low-cost technologies for photovoltaic purposes.⁸ Nevertheless, the stability of the devices in ambient conditions and in operation is undesirably poor, and many efforts have been made to overcome this major drawback.

The first PSCs were based on methylammonium lead iodide perovskite (MAPbI₃), after the work of Miyasaka and co-workers,⁹ and the poor stability of this composition is mainly due to a thermal decomposition process during operation conditions.¹⁰⁻¹² Later works started employing formamidinium (FA) and cesium (Cs) cations, or a mixture of them, and the devices benefited from the mixture. The fact that Cs and FA are not easily removed from the structure and the larger mixture entropy of the mixed cations yielded a perovskite with improved stability, charge-carrier transport, and, consequently, efficiency. In addition, beyond the A-site cation mixture, the mixed halide perovskites, AB(Br/I)₃ (A = Cs⁺, FA⁺, or methylammonium (MA⁺); B = Pb²⁺ or Sn²⁺; Figure 1a), showed further improvement in performance.¹³⁻¹⁷ Currently, the most commonly used perovskite composition is the mixed cation (CsFAMA)Pb(Br/I)₃, and the best devices present over 20% efficiency.¹⁸ However, although improvements have been made, these PSCs still suffer from poor stability, which remains as one of the main challenges in the field.

Currently, there are two noticeable strategies to overcome this issue: passivation of defects¹⁹⁻²¹ and the use

*e-mail: flaraujo@unicamp.br; anafla@unicamp.br
Editor handled this article: Luiz Ramos (Guest)

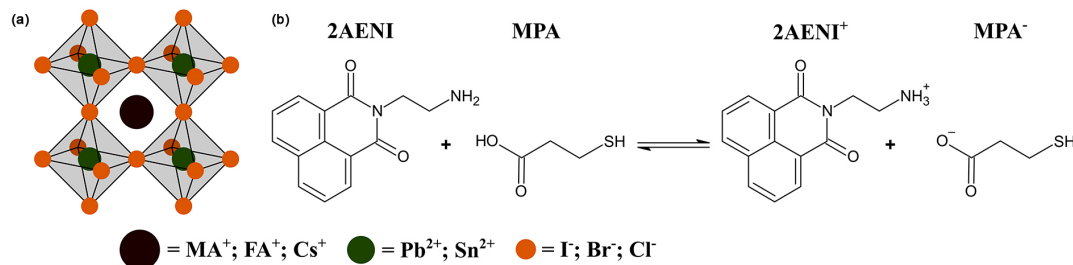


Figure 1. (a) Schematic representation of a general perovskite and its various compositions; (b) reaction between 2AENI and MPA.

of bulkier (mono)diammonium cations to form a 2D/3D interface.^{22,23} In the former, better device performance and stability are achieved, in general, due to increase in carriers' lifetime and charge mobility as a consequence of defect passivation, and a series of strategies can be used for this purpose.^{21,24,25} Also, passivation helps avoid ion migration and phase segregation in mixed-cation, mixed-halide perovskites (CsFAMA, for simplicity), which is a serious issue regarding their stability.²⁶⁻²⁸ The strategy of using bulkier ammonium cations can both passivate defects and form a 2D layer on the surface of the perovskite, or an intermixed 2D/3D layer. The bulky carbon chains from the ammonium cations offer a higher moisture stability, also preventing ion migration and phase segregation; however, the alkyl chains are insulating, which normally hinders charge transport.^{25,29} Having in mind these two approaches, we prepared a combination of two molecules with potential for passivation of defects and stabilization of CsFAMA perovskites.

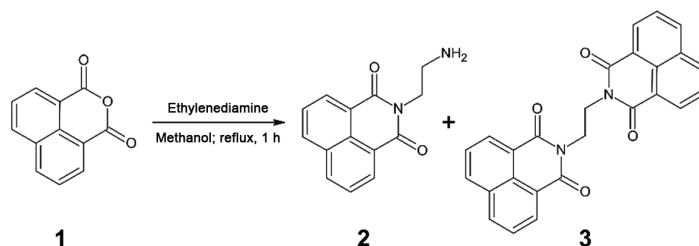
In this work, we synthesize the molecule *N*-(2-aminoethyl)naphthalimide (2AENI) and combined it with mercaptopropionic acid (MPA) (Figure 1b), demonstrating that this combination can improve the stability of the perovskite films and PSCs in ambient conditions. We chose these two molecules (2AENI + MPA) as complementary moieties. The presence of MPA in the same solution allows the protonation of the 2AENI primary amine, facilitating its interaction with the perovskite in the A-site vacancies, although the neutral molecule could also interact with the perovskite. Also, MPA alone is a bidentate ligand, having a thiol and a carboxylate group, which can interact with Pb²⁺ cation in the surface and grain boundaries of CsFAMA.³⁰

Our modification does not influence significantly in the performance of the devices. To date, 2AENI-MPA has not yet been applied to this purpose, to the best of our knowledge, although a similar molecule has been introduced in 2D perovskites, demonstrating potential for charge transport between organic and inorganic layers.³¹ As such, this work introduces a new approach for the stabilization of CsFAMA perovskite, using a post-treatment protocol with an unexplored combination of two molecules.

Results and Discussion

The synthesis of the 2AENI molecule is carried out through the reaction of 1,8-naphthalic anhydride (**1**) and ethylenediamine, as shown in the Scheme 1. Since the reaction is carried out in excess of ethylenediamine, this reaction condition favors the formation of **2**. However, the formation of the disubstituted byproduct is difficult to avoid, and our synthesis yields a ratio of 98% of **2** and 2% of **3** (molar ratio). The two products are separated by silica gel chromatography, and the purified product was used in association with MPA to modify the perovskite films. For more details on the synthesis, see the Experimental section.

The CsFAMA perovskite films were fabricated following well-known, established protocols,¹⁸ and the modification of the films was carried out in a similar approach recently published by our group.²⁰ Briefly, the films were modified with an isopropanol (IPA) solution containing 2AENI and MPA with different concentrations: neat IPA, 1, 2.5, 5, and 10 mM. The X-ray diffraction (XRD) pattern of the perovskite and the scanning electron microscopy (SEM) images of the films are shown in



Scheme 1. Synthesis reaction of *N*-(2-aminoethyl)naphthalimide (2AENI).

Figures 2a and 2b. In terms of crystalline structure, from the diffractograms perspective, the modification of the films with 2AENI-MPA does not cause any visible change. It is noteworthy that the PbI_2 peak in the diffractogram comes from the white crystallites^{32,33} observable in the SEM images due to an intended excess of PbI_2 (9%)³⁴ used during the perovskite deposition. Since PbI_2 is a lamellar material, its orientation regarding the substrate influences in the intensity of this peak in the diffractogram. From the SEM perspective, films show an increasing smoothness as the concentration of 2AENI-MPA increases. This behavior is consistent to the deposition of the 2AENI-MPA molecules on the surface of the film. The effect is more evident in sample modified with the 10 mM solution, where the grain boundaries are not clear due to a larger material deposition. Figure S1 (Supplementary Information (SI) section) shows a comparison of the Fourier transform infrared (FTIR) spectra from the 2AENI molecule, the perovskite modified with 10 mM of 2AENI-MPA solution, and the pristine CsFAMA perovskite. A comparison of the FTIR spectra shows that our post-treatment method is effective to deposit the 2AENI molecule on the surface of the perovskite film, in accordance with SEM analysis.

The impact of modification on the optical properties of the materials was evaluated by different electronic spectroscopy techniques. In the UV-Vis absorption spectroscopy (Figure 3a), no difference is observable in the absorption onset of the films upon modification, and the optical bandgap is consistent with previous works.^{20,35} The steady-state PL (SSPL) of the films (Figure 3b) suffer a notorious change: as the concentration of the passivating agent increases, the emission intensity decreases. This change can be explained in terms of a filter effect: the molecule 2AENI has an important absorption band in the

region of the excitation (365 nm, Figure S2a, SI section), which probably acts as a filter for part of the photons from the excitation source. Hence, with less photons reaching the perovskite, its emission intensity decreases proportionally with the concentration of 2AENI-MPA molecules on its surface. Interestingly, although 2AENI has a notorious blue emission (Figure S2b, SI section), its emission cannot be seen in the SSPL of the films, even in the highest concentration of 10 mM. This observation suggests a quenching of the molecule luminescence when it is on the surface of CsFAMA perovskite. To gain more insight into the carriers' dynamics, we measured time-correlated single-photon counting (TCSPC) of the control and modified films, Figure 3c.

To fit the curves from Figure 3c, a three-exponential equation was necessary. When fitting the data with a biexponential (Figure S3, SI section), the chi-square is slightly high and the residual analysis showed a small tendency in short sample-response times, suggesting the necessity of an additional exponential term. However, a multiexponential dynamics is reasonable for these perovskites since they present several recombination mechanisms such as bimolecular, trap-assisted, Auger, and surface/grain-boundary recombination.^{36,37} The complexity of these processes increases with the presence of a high density of trap-states, film disordering, and polycrystalline behavior (Figure 2b) due to the solution-processable deposition by spin-coating method.³⁸⁻⁴¹

In summary, our TCSPC analysis (Figure 3c) shows a continuous decrease in the average lifetime ($\langle\tau\rangle$) with the increase of the 2AENI-MPA concentration in the modification solution, compared to the control sample. Only a considerable increase is observed for the sample with 5 mM when compared with the control and other

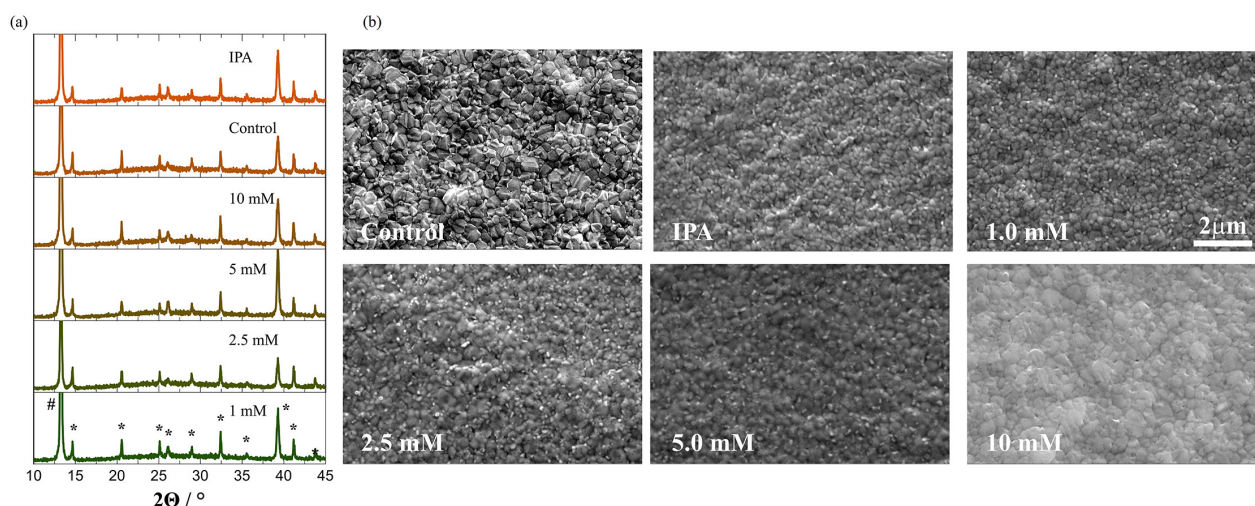


Figure 2. (a) XRD patterns of the films varying the concentration of passivating molecules (* denotes the peaks from the perovskite and # denotes a peak from PbI_2); (b) SEM images of the films with 20,000 \times magnification (the scale bar on the top right is the same for all images).

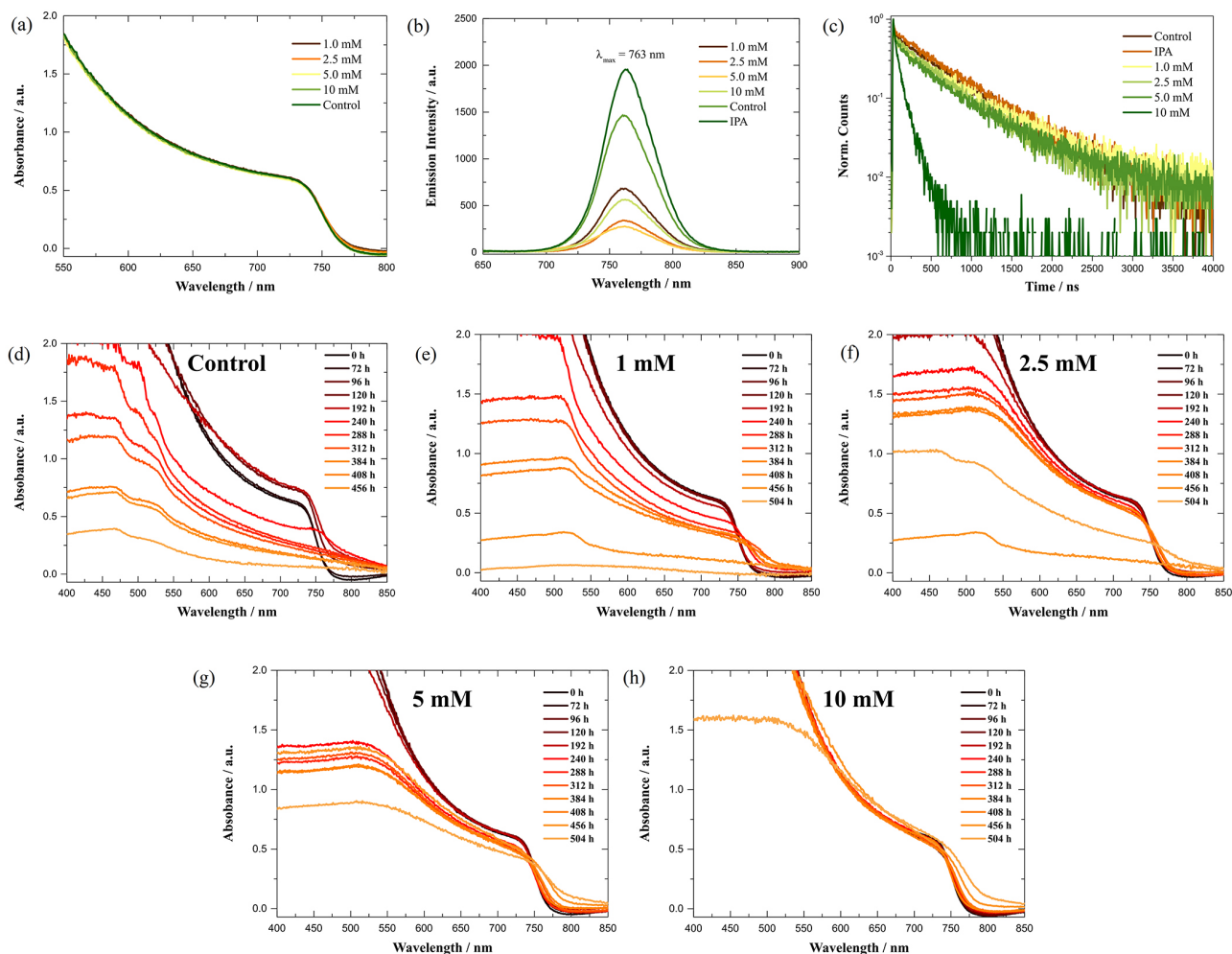


Figure 3. (a-c) Absorption, SSPL, and TCSPC spectra of the films with different modification conditions; (d-h) absorption spectra of the films as function of time under ambient conditions.

passivated perovskite films. This behavior impacts directly on the PSCs figures of merit, mainly in the open-circuit voltage (V_{oc}), hysteresis and, finally, in the stability, as we observed on its photovoltaic device and discuss next. The fitting details of the decays can be found in Figures S4-S9 (SI section), and the parameters extracted from the fits are summarized in Table 1. This little increase in $\langle \tau \rangle$ with 5 mM of 2AENI-MPA can be attributed to a maximization of the passivating effect with 5 mM concentration. In contrast, the general decrease in the lifetime of the charge carriers of the other modified films suggests an increasingly faster charge extraction from the perovskite to the 2AENI molecule,⁴² similar to what is observed when spiro-OMeTAD or an electron transport material is deposited on CsFAMA perovskites.²⁰ A shorter lifetime is generally detrimental for solar cells because charge carriers recombine faster, decreasing the time available for charge collection. This decrease in lifetime is compensated by the passivation of the active layer, and devices do not show an appreciable change in performance.

A significant increase in the stability of the films is observed upon modification with 2AENI-MPA molecules. To verify this effect, we measured the absorption spectra of the films in different times throughout 21 days under ambient conditions, and the results are summarized in Figures 3d-3h. Clearly, the films with treatment degraded more slowly when compared to films with no treatment (with neat IPA), as can be seen from the changes in the absorption onset of the absorption spectra. This trend in degradation and its mechanisms have been carefully investigate in a recent work published by our group.³⁵ It is worth noting that all the spectra were collected in regions close to the center of the films, so that spinner effects on the corner of the substrates were avoided. Visual evidence of the higher stability of the films upon 2AENI-MPA treatment is depicted in Figure S10 (SI section). The variation in ambient humidity and temperature during the survey is shown in Figure S11 (SI section).

To evaluate the effect of the modification on the performance of the solar cells, we prepared devices

Table 1. Parameters of the TCSPC analysis of the perovskite films fitted with a three-exponential equation of the form: $I(t) = A + B_1 e^{-t/\tau_1} + B_2 e^{-t/\tau_2} + B_3 e^{-t/\tau_3}$, where A is a background

Sample	τ_1 / ns	B_1	τ_2 / ns	B_2	τ_3 / ns	B_3	χ^2	$\langle\tau\rangle$ / ns
Control	8.840	0.02	334.690	0.18	720.260	0.80	1.076	683.576
IPA	11.323	0.03	287.264	0.08	690.538	0.89	1.102	675.648
1.0 mM	5.871	0.04	106.867	0.03	667.017	0.93	1.030	663.889
2.5 mM	7.485	0.03	208.962	0.08	574.752	0.89	1.015	562.940
5.0 mM	9.193	0.06	289.148	0.31	803.294	0.63	1.100	725.268
10 mM	13.067	0.12	51.974	0.39	124.422	0.49	1.099	104.579

IPA: isopropanol; τ_1 , τ_2 , and τ_3 : lifetimes of each component; B_1 , B_2 , and B_3 : pre-exponential factors of each component; χ^2 : chi-square value for goodness of fit; $\langle\tau\rangle$: average lifetime of a given decay curve.

with all different concentrations of the modifying agents (see Experimental section for details). We fabricated six devices for each condition to compare their performance and stability. The statistical distributions of photovoltaic parameters for each condition are shown in Figure 4,

and their corresponding values are listed in Table S1 (SI section). The current vs. potential (J-V) curves of the best devices are shown in Figure S12 (SI section), and the best devices' parameters are summarized in Table S1.

The PCE of the devices seems to follow the trend in

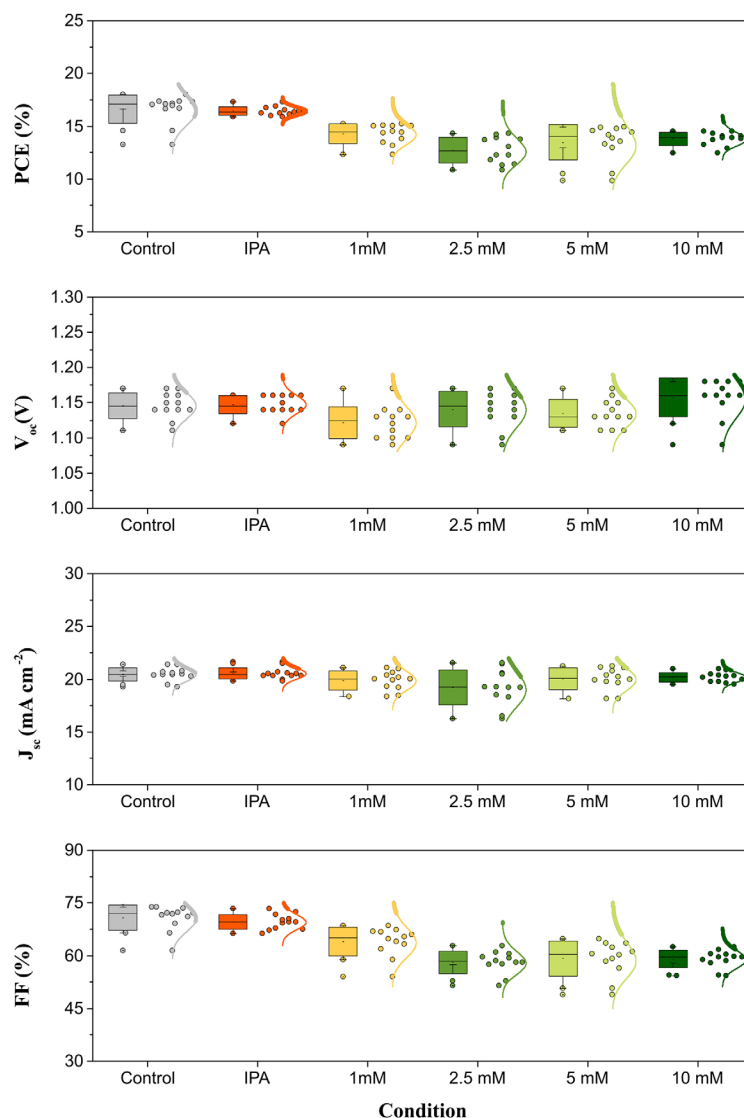


Figure 4. Statistical distributions (reverse and forward scans) of PCE, V_{OC} , J_{SC} , and FF obtained from six perovskite devices for each condition.

the fill-factor (FF). This monotonic decrease in the FF is probably due to the increasing deposition of the bulky 2AENI molecule on the surface of the perovskite as we increase the concentration of the treatment solutions. The presence of the molecules on the surface probably hinders the interface between the perovskite and spiro layers. Interestingly, the device with 10 mM solution treatment does not show a much poorer performance, as one could expect from the short $\langle\tau\rangle$. The reason for this is probably a balance between the effect of lifetime shortening and defect passivation with increasing concentration of 2AENI-MPA. Evidence of this hypothesis is in Figure 3b, where the emission intensity from the film with 10 mM treatment is higher than its 2.5- and 5.0-mM counterparts. Also, the highest open-circuit voltage (V_{oc}) is achieved for the devices with 10 mM of 2AENI-MPA treatment, which is a clear indication of passivation.^{43,44}

The devices with the best performance and reproducibility were the IPA-treated ones. This improvement is in accordance with the higher SSPL intensity and high $\langle\tau\rangle$. Apparently, IPA renormalizes the surface of the film, which probably decreases the density of defects on the surface

and, therefore, device's performance. Similar conclusions have been reported in the literature.^{45,46} Despite the higher reproducibility with neat IPA treatment, these devices do not show any improvement in stability.

The non-encapsulated PSCs were submitted to stability test for 500 h. Our stability test meets the requirements for a first-level International Summit on Organic Photovoltaic Stability (ISOS-D) protocol for ambient conditions in a laboratory environment and lighting.⁴⁷ J-V measurements (under 100 mW cm⁻² illumination, 1 sun) were performed periodically. In Figure 5a, we show the evolution of the PCE values of the PSCs during the period of the tests. We observe that, among the modification of the CsFAMA perovskite layer used, the PSCs with post-treatment with the 5mM solution of 2AENI-MPA showed a better stability up to 500 h of exposure to environmental conditions, retaining around 90% of the initial efficiency. In contrast, the control device retained only 58% of the PCE after the same period. Importantly, our results demonstrate that there is no necessary correlation between a higher stability of the materials (CsFAMA alone) with a higher performance of the devices. Also, although the treatment showed a

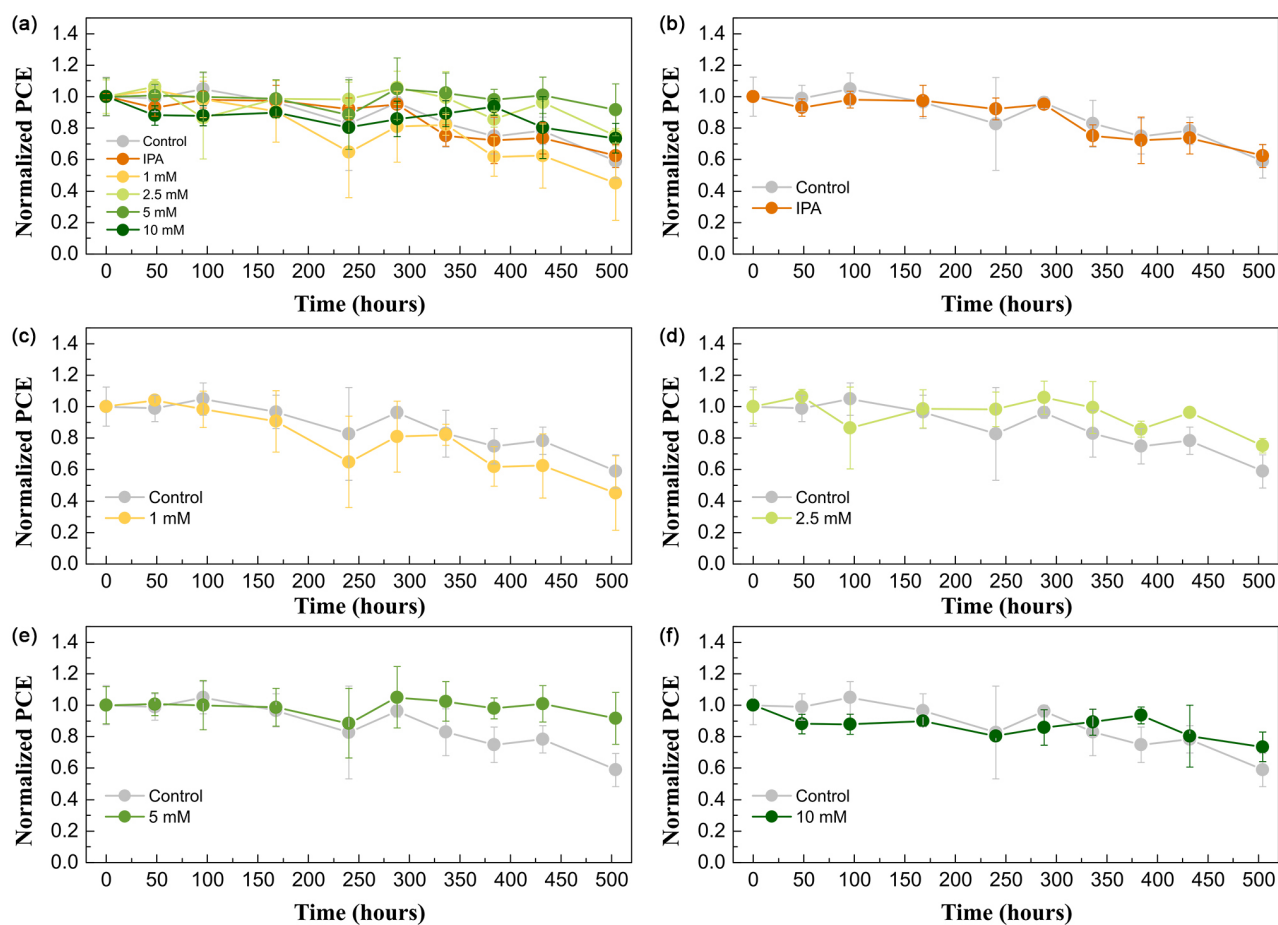


Figure 5. Stability survey of CsFAMA perovskite solar cells with and without 2AENI-MPA modification; the devices were exposed to a laboratory ambient conditions throughout 500 h.

remarkable improvement in the stability of the perovskite on glass (Figures 3d-3h), the device stability does not seem to improve in the same extent (Figures 5b-5f). This observation is important to show that a higher material stability may be only partially transferred to devices, which is expected, since, during the operation of solar cells, a series of different stress conditions such as ambient humidity, illumination, bias voltage can cause uncountable chemical modifications between/within the different layers of the devices.

Conclusions

In this work we demonstrate that the combination of *N*-(2-aminoethyl)naphthalimide (2AENI) with mercaptopropionic acid (MPA) improve the stability of CsFAMA perovskite and their respective solar cells. The deposition of the 2AENI molecule seem to impact on the interface between perovskite and spiro, causing a monotonic decrease in the FF and, with exception of the 5 mM condition, a decrease in $\langle \tau \rangle$. The modification proposed does not influence considerably in the performance of the devices. Our work emphasizes the importance of designing new molecules with passivating purposes in the field of perovskite solar cells such as *N*-(2-aminoethyl)naphthalimide. Molecules capable of passivating films while offering an efficient charge transfer/collection is an important avenue for the current stability issue faced by the perovskite-based photovoltaics. A possible way to accomplish this goal is to design a molecule that improves the perovskite/spiro-OMeTAD interface for a better charge collection and transport and, consequently, better device performance.

Experimental

Synthesis of (2-aminoethyl)naphthalimide (2AENI)

The synthesis of the 2AENI was adapted from the literature.⁴⁸⁻⁵⁰ In a 100 mL, round bottom flask, 198.17 mg (1 mmol) of 1,8-naphthalic anhydride (**1**) was dissolved in 25 mL of anhydrous methanol. The mixture was placed in an oil bath with magnetic stirring and allowed to heat up to 60 °C. In a different flask, 1.00 mL (15 mmol) of ethylenediamine was dissolved in 15 mL of anhydrous methanol. The ethylenediamine solution was, then, added slowly (ca. 3 min) to the 1,8-naphthalic anhydride mixture in methanol at 60 °C. A reflux condenser was attached to the reaction flask, and the reaction was allowed to reflux for 1 h. The reaction colors change from a light to a dark yellow.

Upon the reaction completion, products **2** (2AENI) and **3** (disubstituted byproduct) were formed in a

0.98:0.02 molar fraction. The reaction solution was filtered in a paper filter, and the supernatant was dried in a rotatory evaporator to give a yellow/brownish solid. To separate the two products, silica gel column chromatography was used with a mobile phase composed of a mixture of chloroform/methanol (7:3 v/v); the same solvent mixture was used to place the product on the top of the column. The second fraction collected, with a greenish color, is the product of interest, *N*-(2-aminoethyl)naphthalimide (**2**).

Global yield 84%; ¹H NMR (250 MHz, CDCl₃) δ 8.61 (dd, *J* 7.3, 1.0 Hz, 2H), 8.22 (dd, *J* 8.4, 1.0 Hz, H), 7.76 (dd, *J* 8.3, 7.3 Hz, 2H), 4.29 (t, *J* 6.6 Hz, 2H), 3.07 (t, *J* 6.6 Hz, 2H), 1.33 (s, 2H); UV-Vis (methanol) λ / nm 232, 330; ESI-MS *m/z*, (%): 241.09 (688) [M + H]⁺. UV-Vis, ¹H nuclear magnetic resonance (NMR), and mass spectra are presented in SI section in Figures S2, S13, and S14, respectively.

Perovskite precursor solution

CsFAMA (Cs_{0.05}FA_{0.85}MA_{0.10}Pb(I_{0.83}Br_{0.17})₃) perovskite solution was prepared according to the protocol described by Saliba *et al.*¹⁸ The stock solutions were prepared separately, according to Table 2.

Table 2. Solutions to prepare the precursor solution of CsFAMA perovskite

Solution	Mass / mg	Solvent/solution
PbI ₂	1240	1.8 mL of DMF:DMSO (4:1 v/v)
PbBr ₂	275	0.5 mL of DMF:DMSO (4:1 v/v)
CsI	117	0.3 mL de DMSO
FAI	385	1.8 mL of PbI ₂ solution
MABr	56.8	0.4 mL of PbBr ₂ solution

FAI: formamidinium iodide; MABr: methylammonium bromide; DMF: dimethylformamide; DMSO: dimethyl sulfoxide.

The solutions of PbI₂ and PbBr₂ were agitated at 180 °C for 10 min. After this time, the solutions of PbI₂, PbBr₂, and CsI were agitated at 150 °C for 10 min. At last, the solutions were kept under agitation for 1 h at 100 °C. After stirring under heat, these solutions cooled down to room temperature, and the solutions of FAPbI₃ and MAPbBr₃ were prepared by dissolving FAI and MABr according to Table 2 and keeping them under agitation in room temperature for 1 h. After that, to prepare the perovskite precursor solution, we mixed 1.75 mL of FAPbI₃ solution, 0.35 mL of MAPbBr₃ solution, and 0.112 mL of CsI solution. This precursor solution was stirred for an additional 30 min. The final concentration of the solution (CsFAMA) is 1.5 M.

Modification solution-2AENI + MPA

Precursor solution of 2AENI + MPA was prepared by mixing 4.5 μL of mercaptopropionic acid (0.052 mmol) in 5 mL of anhydrous isopropanol (concentration = 10.3 mM). After the mixture, 12.0 mg of 2AENI (0.05 mmol) was added to the solution (concentration of 2AENI = 10.0 mM), and the mixture was stirred at 60 °C for 30 min. After complete dissolution of 2AENI, the solution was filtered with a PTFE (polytetrafluoroethylene) hydrophilic syringe filter (45 μm) and transferred to a N_2 filled glovebox and three other dilutions were prepared from this precursor: 5 mM (1:1 v/v with isopropanol), 2.5 mM (1:3 v/v with isopropanol), and 1 mM (1:9 v/v with isopropanol).

Film deposition and device fabrication

The devices were prepared on a fluorine-doped tin oxide substrate deposited on glass (FTO) with the following architecture: glass/FTO/ SnO_2 /KCl/CsFAMA/Spiro-OMeTAD/Au. The modification of the devices was carried out before the deposition of spiro-OMeTAD. FTO substrates were immersed in Hellmanex® 2% (v/v) in deionized water and placed in a sonicator bath for 20 min. This sonication step was, then, repeated with pure deionized water, acetone, and isopropanol.

SnO_2 deposition

Before the deposition of SnO_2 , the substrates were dried and treated with UV-ozone for 20 min. A 0.05 M solution of $\text{SnCl}_4 \cdot 5\text{H}_2\text{O}$ in isopropanol was spin-coated on the FTO substrates at 3000 rpm for 36 s and acceleration of 500 rpm s^{-1} . The films were treated at 180 °C for 1 h to convert the $\text{SnCl}_4 \cdot 5\text{H}_2\text{O}$ into SnO_2 . The SnO_2 films received a new UV-ozone treatment for 20 min, and a 10 mM KCl solution in deionized water (100 μL) was spin-coated on the SnO_2 films at 3000 rpm for 30 s and acceleration of 2000 rpm s^{-1} . After this deposition, the films were thermally treated at 100 °C for 10 min.

Perovskite deposition

Before the deposition of the perovskite layer, the films were treated again under UV-ozone for 20 min. To deposit the perovskite, 50 μL of the precursor solution were spin-coated at 1000 rpm for 10 s, with acceleration of 200 rpm s^{-1} , and then 6000 rpm for 20 s, with acceleration of 2000 rpm s^{-1} . After 10 s at 6000 rpm, 200 μL of chlorobenzene was dropped on the spinning substrate as the antisolvent. The resulting perovskite films were thermally treated at 100 °C for 30 min. From these films, we prepared control and modified devices.

Device modification and control

We made two types of control devices; one without any modification, using the perovskite film as prepared; and the other with neat IPA treatment. The deposition of the modifying solution was made as follows: 50 μL of the solution at a given concentration (0, 1.0, 2.5, 5.0, and 10 mM) were spin-cast on the spinning substrate at 3000 rpm and it was allowed to spin for 30 s. The modified films were then submitted to a thermal treatment at 100 °C for 30 min.

Spiro-OMeTAD solution and deposition

The concentration of the solution is 70 mM of spiro-OMeTAD in chlorobenzene. 200 mg of spiro-OMeTAD were dissolved in 2 mL of anhydrous chlorobenzene. This solution was allowed to stir or 30 min at room temperature. Sequentially, the common additives were added to the solution: 72 μL of *tert*-butyl pyridine, 40 μL of bis(trifluoromethane)sulfonimide lithium salt (LITFSI, 1.8 mol L^{-1} in acetonitrile), and 16 μL of cobalt complex FK209 (0.25 mol L^{-1} in acetonitrile). A volume of 50 μL of solution was spin-cast on the spinning substrate at 4000 rpm and allowed to spin for 20 s.

Counter electrode

Gold was deposited by thermal evaporation in a two-step process: the first 2 nm at 0.2 $\text{\AA} \text{s}^{-1}$ and then at 1.0 $\text{\AA} \text{s}^{-1}$ up to 80 nm. A shadow mask was used to define the cell area (0.25 cm^2).

Materials

Lead iodide (PbI_2 , 99.99%), cesium iodide (CsI, 99.9%), and lead bromide (PbBr_2 , 99.99%) were purchased from TCI America, 9211 N. Harborgate St., Portland, OR 97203, USA. 4-*tert*-Butylpyridine (tBP; 98%), lithium bis(trifluoromethanesulfonyl)imide (LiTFSI; 99.95%), tin(IV) chloride pentahydrate ($\text{SnCl}_4 \cdot 5\text{H}_2\text{O}$), and anhydrous solvents (dimethyl formamide (DMF), dimethyl sulfoxide (DMSO), isopropanol (IPA), acetonitrile and chlorobenzene), and potassium chloride solution (KCl) were purchased from Sigma-Aldrich, São Paulo, Brazil. Methanol (99.9%) was purchased from Synth, São Paulo, Brazil. Formamidinium iodide (FAI), methylammonium bromide (MABr), tris(2-(1*H*-pyrazol-1-yl)-4-*tert*-butylpyridine)cobalt(III)tri[bis(trifluoromethane)sulfonimide] (FK209 Co(III) TFSI), and FTO coated glasses substrate (TEC7, 300 mm \times 300 mm \times 2.2 mm) were supplied by GreatCell Solar LTD, Queanbeyan, Australia. Spiro-OMeTAD (2,2',7,7'-tetrakis(*N,N*-di-*p*-methoxyphenylamine)9,9'-spirobifluorene) were purchased from Xi'an

Polymer Light Technology Corp. Naphthalic anhydride and ethylene diamine (ReagentPlus®, ≥ 99%) were purchased from Sigma-Aldrich, São Paulo, Brazil.

Equipment and characterizations

TCSPC

The charge carrier dynamics of the modified and non-modified films were recorded using time-correlated single-photon counting in a Edinburg Analytical Instruments FL 900 spectrofluorometer with an MCP-PMT (Hamamatsu R3809U-50; 50 ps) with a PicoQuant LDH-D-C-440 pulsed diode laser operating at $\lambda_{exc} = 440$ nm (bandwidth of 5 nm, pulsewidth = 80 ps; laser fluence, $F = 9.7$ nJ cm⁻²). The decay signals were collected at the maxima emission wavelength of each sample in a time scale of 2 μ s. The instrument response was recorded using a Ludox sample.

Fourier transform infrared spectroscopy

The spectrum was acquired through a Cary 630 FTIR spectrometer using attenuated total reflectance (ATR) acquisition mode. To increase the reflectance signal of the spectra, we deposited the films on a silicon substrate coated with 80 nm of gold.

Absorption spectra

Absorbance in thin films was measured in Agilent Carry 60 UV-Vis equipment in the transmission mode. A glass substrate was used as the baseline for all the spectra.

Photoluminescence spectra

Measurements were performed in an Ocean Optics QEPro spectrofluorometer with and 365 nm LED as an excitation light source directly on the surface of the films. The excitation power was 2.6 mW cm⁻².

SEM

The scanning electron microscopy images were obtained on a Thermo Fisher Scientific Quanta™ 250 FEG-SEM at 5 kV, under high vacuum (1.24×10^{-4} Pa), a magnification of 20.000 \times , and with an Everhart Thornley Detector (ETD).

XRD

Diffraction patterns were registered in a Shimadzu XRD-7000 with a Cu K α source (1.54 Å). The scanning step was 0.02 2 θ° with a scan speed of 2° s⁻¹.

¹H nuclear magnetic resonance (NMR)

Spectra were recorded using a Bruker Avance III HD 250 MHz spectrometer, using chloroform-*d* (CDCl₃) as a

solvent; chemical shifts were compared with an internal reference, tetramethylsilane (TMS).

Mass spectrometry

Mass spectrometry was recorded in a Orbi-Trap Thermo Q-Exactive equipment at positive ionizing mode. 1 mg of *N*-(2-aminoethyl)naphthalimide was dissolved in methanol and water (1:1 v/v).

Current-voltage characteristics

J-V curves of the PSCs were measured using a source-meter (Keithley 2400 SourceMeter), in a voltage range from 0 to 1.2 V (forward scan) and +1.2 to 0 V (reverse scan) with steps of 10 mV and delay time of 0.25 s. A class AAA Solar Simulator (AM 1.5G, HAL-320, Asahi Spectra Co., Ltd.) was used for the J-V measurements under illumination, and the light intensity was calibrated by using a silicon reference solar cell with a KG5 filter. Active area (area under illumination) was defined using a shadow mask (0.12 cm²) during JV measurement.

Supplementary Information

Supplementary information (2AENI characterization, TCSPC decays fit, J-V curves of the solar cells, degradation survey) is available free of charge at <http://jbcs.sbg.org.br> as PDF file.

Acknowledgments

A.F.N., F.L.A., and P.E.M gratefully acknowledge support from FAPESP (the São Paulo Research Foundation, process 2017/11986-5) and Shell and the strategic importance of the support given by ANP (Brazil's National Oil, Natural Gas and Biofuels Agency) through the R&D levy regulation. F. L. A. acknowledges FAPESP (process 2020/14451-8). R.F.M. acknowledges FAPESP (process 2019/25765-6). A.B.H. acknowledges CNPq grants under the process numbers: 122874/2020-0 and 116430/2019-2. J. C. G. acknowledges i3N, UIDB/50025/2020 and UIDP/50025/2020, financed by national funds through the FCT/MEC. L. G. B. thanks to FAPESP (process 2021/13262-0). We thank Rodrigo Szostak and Bruno Leuzinger da Silva for the J-V curve software development and for the help with SEM measurements, respectively.

Author Contributions

Conceptualization (RFM, FLA, JCG, LGB), data curation (RFM, ABH, FLA), formal analysis funding acquisition (RFM, FLA, AFN), investigation (RFM, FLA, ABH, PEM), project administration

(RFM, FLA, AFN), resources (AFN), validation (RFM, ABH, FLA), visualization (RFM, FLA, PEM), writing original draft (RFM), writing review and editing (all authors).

References

1. Tollefson, J.; *Nature* **2019**, *574*, 17.
2. Teske, S.; *Achieving the Paris Climate Agreement Goals*; Springer International Publishing: Cham, 2019.
3. Aranda, C. A.; Caliò, L.; Salado, M.; *Crystals* **2021**, *11*, 519.
4. Raphael, E.; Silva, M.; Szostak, R.; Schiavon, M. A.; Nogueira, A. F.; *Quim. Nova* **2018**, *41*, 61.
5. Han, G. S.; Jung, H. S.; Park, N.-G.; *Chem. Commun.* **2021**, 57, 11604.
6. Green, M. A.; Dunlop, E. D.; Hohl-Ebinger, J.; Yoshita, M.; Kopidakis, N.; Hao, X.; *Prog. Photovoltaics* **2021**, *29*, 657.
7. National Renewable Energy Laboratory (NREL); *Best Research-Cell Efficiency Chart*, <https://www.nrel.gov/pv/cell-efficiency.html>, accessed in May 2022.
8. Dunlap-Shohl, W. A.; Zhou, Y.; Padture, N. P.; Mitzi, D. B.; *Chem. Rev.* **2019**, *119*, 3193.
9. Kojima, A.; Teshima, K.; Shirai, Y.; Miyasaka, T.; *J. Am. Chem. Soc.* **2009**, *131*, 6050.
10. Conings, B.; Drijkoningen, J.; Gauquelin, N.; Babayigit, A.; D'Haen, J.; D'Olieslaeger, L.; Ethirajan, A.; Verbeeck, J.; Manca, J.; Mosconi, E.; de Angelis, F.; Boyen, H.-G.; *Adv. Energy Mater.* **2015**, *5*, 1500477.
11. Akbulatov, A. F.; Luchkin, S. Y.; Frolova, L. A.; Dremova, N. N.; Gerasimov, K. L.; Zhidkov, I. S.; Anokhin, D. V.; Kurmaev, E. Z.; Stevenson, K. J.; Troshin, P. A.; *J. Phys. Chem. Lett.* **2017**, *8*, 1211.
12. Latini, A.; Gigli, G.; Ciccio, A.; *Sustainable Energy Fuels* **2017**, *1*, 1351.
13. Yi, C.; Luo, J.; Meloni, S.; Boziki, A.; Ashari-Astani, N.; Grätzel, C.; Zakeeruddin, S. M.; Röthlisberger, U.; Grätzel, M.; *Energy Environ. Sci.* **2016**, *9*, 656.
14. Saliba, M.; Matsui, T.; Seo, J.-Y.; Domanski, K.; Correa-Baena, J.-P.; Nazeeruddin, M. K.; Zakeeruddin, S. M.; Tress, W.; Abate, A.; Hagfeldt, A.; Grätzel, M.; *Energy Environ. Sci.* **2016**, *9*, 1989.
15. Ünlü, F.; Jung, E.; Haddad, J.; Kulkarni, A.; Öz, S.; Choi, H.; Fischer, T.; Chakraborty, S.; Kirchartz, T.; Mathur, S.; *APL Mater.* **2020**, *8*, 070901.
16. Caetano, C.; Butler, K. T.; Walsh, A.; *Phys. Rev. B* **2016**, *93*, 144205.
17. Butler, K. T.; Walsh, A.; Cheetham, A. K.; Kieslich, G.; *Chem. Sci.* **2016**, *7*, 6316.
18. Saliba, M.; Correa-Baena, J.-P.; Wolff, C. M.; Stolterfoht, M.; Phung, N.; Albrecht, S.; Neher, D.; Abate, A.; *Chem. Mater.* **2018**, *30*, 4193.
19. Liu, C.; Sun, J.; Tan, W. L.; Lu, J.; Gengenbach, T. R.; McNeill, C. R.; Ge, Z.; Cheng, Y.-B.; Bach, U.; *Nano Lett.* **2020**, *20*, 1240.
20. Germino, J. C.; Szostak, R.; Motti, S. G.; Moral, R. F.; Marchezi, P. E.; Seleghini, H. S.; Bonato, L. G.; de Araújo, F. L.; Atvars, T. D. Z.; Herz, L. M.; Fenning, D.; Hagfeldt, A.; Nogueira, A. F.; *ACS Photonics* **2020**, *7*, 2282.
21. Gao, F.; Zhao, Y.; Zhang, X.; You, J.; *Adv. Energy Mater.* **2020**, *10*, 1902650.
22. Sutanto, A. A.; Szostak, R.; Drigo, N.; Queloz, V. I. E.; Marchezi, P. E.; Germino, J. C.; Tolentino, H. C. N.; Nazeeruddin, M. K.; Nogueira, A. F.; Grancini, G.; *Nano Lett.* **2020**, *20*, 3992.
23. de Holanda, M. S.; Szostak, R.; Marchezi, P. E.; Duarte, L. G. T. A.; Germino, J. C.; Atvars, T. D. Z.; Nogueira, A. F.; *Sol. RRL* **2019**, *3*, 1900199.
24. Correa-Baena, J. P.; Luo, Y.; Brenner, T. M.; Snider, J.; Sun, S.; Li, X.; Jensen, M. A.; Hartono, N. T. P.; Nienhaus, L.; Wieghold, S.; Poindexter, J. R.; Wang, S.; Meng, Y. S.; Wang, T.; Lai, B.; Holt, M. V.; Cai, Z.; Bawendi, M. G.; Huang, L.; Buonassisi, T.; Fenning, D. P.; *Science* **2019**, *363*, 627.
25. Liu, G.; Zheng, H.; Xu, X.; Xu, S.; Zhang, X.; Pan, X.; Dai, S.; *Adv. Funct. Mater.* **2019**, *29*, 1807565.
26. Cao, J.; Tao, S. X.; Bobbert, P. A.; Wong, C.-P.; Zhao, N.; *Adv. Mater.* **2018**, *30*, 1707350.
27. Cho, J.; Kamat, P. V.; *Chem. Mater.* **2020**, *32*, 6206.
28. Wei, J.; Wang, Q.; Huo, J.; Gao, F.; Gan, Z.; Zhao, Q.; Li, H.; *Adv. Energy Mater.* **2021**, *11*, 2002326.
29. Ma, C.; Shen, D.; Ng, T.-W.; Lo, M.-F.; Lee, C.-S.; *Adv. Mater.* **2018**, *30*, 1800710.
30. Wang, N.; Zhao, K.; Ding, T.; Liu, W.; Ahmed, A. S.; Wang, Z.; Tian, M.; Sun, X. W.; Zhang, Q.; *Adv. Energy Mater.* **2017**, *7*, 1700522.
31. Mishra, A.; Ahlawat, P.; Fish, G. C.; Jahanbakhshi, F.; Mladenović, M.; Almalki, M.; Ruiz-Preciado, M. A.; Gelvéz-Rueda, M. C.; Kubicki, D. J.; Schouwink, P. A.; Dufoulon, V.; Schneeberger, T.; Aslanzadeh, A.; Grozema, F. C.; Zakeeruddin, S. M.; Moser, J.; Rothlisberger, U.; Emsley, L.; Milić, J. V.; Grätzel, M.; *Chem. Mater.* **2021**, *33*, 6412.
32. Roose, B.; Dey, K.; Chiang, Y.-H.; Friend, R. H.; Stranks, S. D.; *J. Phys. Chem. Lett.* **2020**, *11*, 6505.
33. Chen, Y.; Meng, Q.; Xiao, Y.; Zhang, X.; Sun, J.; Han, C. B.; Gao, H.; Zhang, Y.; Lu, Y.; Yan, H.; *ACS Appl. Mater. Interfaces* **2019**, *11*, 44101.
34. Bi, D.; Tress, W.; Dar, M. I.; Gao, P.; Luo, J.; Renevier, C.; Schenk, K.; Abate, A.; Giordano, F.; Correa Baena, J.-P.; Decoppet, J.-D.; Zakeeruddin, S. M.; Nazeeruddin, M. K.; Grätzel, M.; Hagfeldt, A.; *Sci. Adv.* **2016**, *2*, e1501170.
35. Marchezi, P. E.; Therézio, E. M.; Szostak, R.; Loureiro, H. C.; Bruening, K.; Gold-Parker, A.; Melo, M. A.; Tassone, C. J.; Tolentino, H. C. N.; Toney, M. F.; Nogueira, A. F.; *J. Mater. Chem. A* **2020**, *8*, 9302.
36. Hages, C. J.; Redinger, A.; Levchenko, S.; Hempel, H.; Koepfer, M. J.; Agrawal, R.; Greiner, D.; Kaufmann, C. A.; Unold, T.; *Adv. Energy Mater.* **2017**, *7*, 1700167.

37. Staub, F.; Hempel, H.; Hebig, J.-C.; Mock, J.; Paetzold, U. W.; Rau, U.; Unold, T.; Kirchartz, T.; *Phys. Rev. Appl.* **2016**, *6*, 044017.
38. Jin, H.; Debroye, E.; Keshavarz, M.; Scheblykin, I. G.; Roeffaers, M. B. J.; Hofkens, J.; Steele, J. A.; *Mater. Horiz.* **2020**, *7*, 397.
39. Johnston, M. B.; Herz, L. M.; *Acc. Chem. Res.* **2016**, *49*, 146.
40. deQuillettes, D. W.; Frohna, K.; Emin, D.; Kirchartz, T.; Bulovic, V.; Ginger, D. S.; Stranks, S. D.; *Chem. Rev.* **2019**, *119*, 11007.
41. Correa-Baena, J.-P.; Turren-Cruz, S.-H.; Tress, W.; Hagfeldt, A.; Aranda, C.; Shooshtari, L.; Bisquert, J.; Guerrero, A.; *ACS Energy Lett.* **2017**, *2*, 681.
42. Said, A. A.; Xie, J.; Zhang, Q.; *Small* **2019**, *15*, 1900854.
43. Zhu, X.; Du, M.; Feng, J.; Wang, H.; Xu, Z.; Wang, L.; Zuo, S.; Wang, C.; Wang, Z.; Zhang, C.; Ren, X.; Priya, S.; Yang, D.; Liu, S. F.; *Angew. Chem., Int. Ed.* **2021**, *60*, 4238.
44. Zhou, Q.; Gao, Y.; Cai, C.; Zhang, Z.; Xu, J.; Yuan, Z.; Gao, P.; *Angew. Chem.* **2021**, *133*, 8384.
45. Wang, X.; Li, X.; Tang, G.; Zhao, L.; Zhang, W.; Jiu, T.; Fang, J.; *Org. Electron.* **2015**, *24*, 205.
46. Chen, D.; Li, X.; Su, A.; Dong, H.; Pang, S.; Zhu, W.; Xi, H.; Zhang, J.; Zhang, C.; Hao, Y.; *Dalton Trans.* **2019**, *48*, 5292.
47. Khenkin, M. V.; Katz, E. A.; Abate, A.; Bardizza, G.; Berry, J. J.; Brabec, C.; Brunetti, F.; Bulović, V.; Burlingame, Q.; Di Carlo, A.; Cheacharoen, R.; Cheng, Y.-B.; Colsmann, A.; Cros, S.; Domanski, K.; Duzza, M.; Fell, C. J.; Forrest, S. R.; Galagan, Y.; Di Girolamo, D.; Grätzel, M.; Hagfeldt, A.; von Hauff, E.; Hoppe, H.; Kettle, J.; Köbler, H.; Leite, M. S.; Liu, S.; Loo, Y.-L.; Luther, J. M.; Ma, C.-Q.; Madsen, M.; Manceau, M.; Matheron, M.; McGehee, M.; Meitzner, R.; Nazeeruddin, M. K.; Nogueira, A. F.; Odabaşı, Ç.; Osherov, A.; Park, N.-G.; Reese, M. O.; de Rossi, F.; Saliba, M.; Schubert, U. S.; Snaith, H. J.; Stranks, S. D.; Tress, W.; Troshin, P. A.; Turkovic, V.; Veenstra, S.; Visoly-Fisher, I.; Walsh, A.; Watson, T.; Xie, H.; Yıldırım, R.; Zakeeruddin, S. M.; Zhu, K.; Lira-Cantu, M.; *Nat. Energy* **2020**, *5*, 35.
48. Licchelli, M.; Biroli, A. O.; Poggi, A.; Sacchi, D.; Sangermani, C.; Zema, M.; *Dalton Trans.* **2003**, 4537.
49. Ledwon, P.; Brzeczek, A.; Pluczyk, S.; Jarosz, T.; Kuznik, W.; Walczak, K.; Lapkowski, M.; *Electrochim. Acta* **2014**, *128*, 420.
50. Lebègue, E.; Benoit, C.; Brousse, T.; Gaubicher, J.; Cougnon, C.; *J. Electrochem. Soc.* **2015**, *162*, A2289.

Submitted: November 4, 2021

Published online: May 11, 2022

